INSTITUTE OF PHYSICS PUBLISHING JOURNAL OF PHYSICS B: ATOMIC, MOLECULAR AND OPTICAL PHYSICS

J. Phys. B: At. Mol. Opt. Phys. **39** (2006) 3781–3790 doi:10.1088/0953-4075/39/18/008

Absorption effects in intermediate energy elastic electron scattering from xenon

H Cho[1], R P McEachran[2], S J Buckman[2], D M Filipović[3,4], V Pejčev[3], B P Marinković[3], H Tanaka[5], A D Stauffer[6] and E C Jung[7]

[1] Physics Department, Chungnam National University, Daejeon 305-764, Korea
[2] AMPL, Australian National University, Canberra, ACT 0200, Australia
[3] Institute of Physics, Pregrevica 118, 11080 Belgrade, Serbia
[4] Faculty of Physics, University of Belgrade, PO Box 386, 11001 Belgrade, Serbia
[5] Physics Department, Sophia University, Chiyoda-ku, Tokyo, Japan
[6] Department of Physics and Astronomy, York University, Toronto M3J 1P3, Canada
[7] Korea Atomic Energy Research Institute, Daejeon 305-600, Korea

Received 24 June 2006
Published 4 September 2006
Online at stacks.iop.org/JPhysB/39/3781

Abstract

We present experimental and theoretical differential cross sections for elastic electron scattering from xenon. Two independent measurements were carried out at (1) Chungnam National University for incident electron energies of 10, 20, 30, 50 and 100 eV and scattering angles from 10° up to 180° and (2) the Institute of Physics in Belgrade for incident electron energies of 20, 30 and 50 eV and scattering angles from 10° up to 150°. While these latter measurements do not cover the full angular range up to 180°, they still extend somewhat higher in scattering angle than previous measurements. It would appear that the theoretical treatment of intermediate energy elastic scattering from xenon is sensitive to the inclusion of absorption effects, particularly at backward scattering angles. This observation plus the previous results for the case of krypton indicates that the role of absorption is generally quite important for the rare gases.

1. Introduction

In a recent paper, Cho *et al* (2004) measured the elastic differential cross section (DCS) from 10° up to 180° for electron scattering from krypton at incident electron energies of 20, 30, 50 and 100 eV, and compared with theoretical calculations, both with and without the inclusion of absorption effects. For those energies, which were above the inelastic threshold of the 5s $[3/2]_2$ state at 9.915 eV for krypton, the experimental results were in best agreement in the backward direction with the theoretical calculation which included absorption effects via a complex optical potential. This optical potential was of the form

$$V(r) = V_{\mathrm{R}}(r) - \mathrm{i}V_{\mathrm{I}}(r) \tag{1}$$

where the real part of the potential (V_R) included both static and dynamic polarization effects, while the imaginary part of the potential ($V_I \geqslant 0$) allowed for flux to be removed from the elastic channel when inelastic processes were energetically possible. Since the potential $V(r)$ is complex, so are the scattering phase shifts $\eta_\kappa = \delta_\kappa + i\gamma_\kappa$ with $\gamma_\kappa \geqslant 0$. Furthermore, the elastic differential cross section was reduced at all scattering angles vis-à-vis the same calculation with $V_I(r) = 0$. Consequently, the total elastic and momentum transfer cross sections are also reduced. In general, γ_κ was only significant for the first few partial waves, i.e., $\gamma_\kappa \to 0$ much more rapidly than $|\delta_\kappa| \to 0$ as $|\kappa|$ increased. The quantum number κ is related to the quantum numbers l and j of the orbital and total angular momenta of the incident electron according to

$$j = |\kappa| - \tfrac{1}{2} \tag{2}$$

and

$$\begin{cases} l = \kappa & \text{if } \kappa > 0 \\ l = -\kappa - 1 & \text{if } \kappa < 0. \end{cases} \tag{3}$$

Thus, it was only those partial waves which corresponded classically to small impact parameters which contributed to the absorption process, as might be expected. However, these are also the partial waves that are most likely to be elastically scattered through large angles. Thus, in an analogous manner to polarization effects, which dominate in the forward scattering direction, absorption effects are expected to manifest strongly in backward scattering. As a result, experiments which measure across the entire angular range, up to 180°, such as those of Cho *et al* (2004), may be ideally suited to provide insight into this effect through a comparison with theoretical calculations, with and without the inclusion of absorption.

However, the above theoretical approach for the optical potential suffered from a basic weakness. In particular, the imaginary part of this optical potential was the local and phenomenological absorption potential of McCarthy *et al* (1977) and hence it contained an overall adjustable and multiplicative parameter $W(E)$. This parameter is energy dependent and is determined by requiring that the total theoretical cross section (elastic plus inelastic) agrees with the average of several experimental measurements of this cross section. In our current study on the heavier noble gas xenon, in which relativistic effects are more important, we have used the *ab initio* optical potential of Chen *et al* (2006) where the imaginary part of the optical potential is now determined from the Dirac–Fock bound and continuum wavefunctions of xenon.

As with other rare gas atoms, there have been many experimental investigations of elastic electron scattering from xenon but only at scattering angles up to around 130°. Among these, the most relevant works include those by Register *et al* (1986), Nishimura *et al* (1987), Ester and Kessler (1994) and Gibson *et al* (1998). On the theoretical side, there have been the reports by McCarthy *et al* (1977), Sienkiewicz and Baylis (1989), Gianturco and Rodriguez-Ruiz (1994), and Johnson and Guet (1994). In this paper, we present experimental and theoretical differential cross sections (DCSs) for elastic electron scattering from xenon. Two independent measurements were carried out at (1) Chungnam National University (CNU) for incident electron energies of 10, 20, 30, 50 and 100 eV and scattering angles from 10° up to 180° and (2) the Institute of Physics (IOP) in Belgrade for incident electron energies of 20, 30 and 50 eV and scattering angles from 10° up to 150°. While the latter measurements do not extend up to 180°, they are still somewhat higher in angular range than previous measurements.

2. Experiments

Since the experimental study is focused on measuring the DCS at backward angles, up to 180°, where cross section measurements are typically inaccessible due to the mechanical constraints of the electron spectrometer, a version of the magnetic-angle-changing device developed by Read and Channing (1996) has been used at CNU, in conjunction with the relative flow technique. Detailed descriptions of the experimental system used at Chungnam National University have been given elsewhere (Cho *et al* 2003a, 2003b), and it is not necessary to repeat all of that detail here. In brief, the xenon target beam is formed by effusion through a single capillary needle with a nozzle diameter of 0.3 mm. This target beam is then crossed with the electron beam produced from the electron monochromator. The overall energy resolution of the spectrometer for the present measurements is about 50–60 meV and the angular resolution of the spectrometer is estimated to be about 1.5°. Relative measurements of the angular distribution are placed on an absolute scale by use of the relative flow technique (Srivastava *et al* 1975). For the present angular differential measurements, we have used the recommended helium elastic differential cross sections of Boesten and Tanaka (1992). The experimental uncertainties in the present DCS vary typically from 7 to 15% and in a few cases are as high as 20%. These uncertainties result from the addition, in quadrature, of statistical errors in the measurements together with the estimated systematic errors of 6–7%. The major source of the systematic errors lies in the uncertainties in the helium cross sections, the electron beam current ratio, the gas pressure ratio and the relative flow rate calibration.

The apparatus used at the Institute of Physics is a conventional crossed beam electron spectrometer. A gas beam generated by a vertical Pt–Ir tube (aspect ratio 0.02) is perpendicularly crossed with a monochromatic incident electron beam. The electrons scattered by xenon into a small solid angle in the horizontal plane were analysed by changing the angle of the analyser around the atomic beam axis from $-30°$ to 150° with respect to the incident electron beam. The analyser optics were optimized to transmit only elastically scattered electrons into a single channel electron multiplier which was used as a detector. In order to achieve this broad angular interval, in spite of the robust mechanical shields that enable differential pumping of the electron optics within the interaction chamber, a special arrangement of the analyser has been designed.

Both the monochromator and analyser were baked in order to prevent the adsorption of gases. The pressure in the chamber without the target gas was 10^{-5} Pa and the background pressure under normal operating conditions was 10^{-3} Pa. A double μ-metal shield reduced the residual magnetic field to less than 0.1 μT in the interaction region. The energy scale was calibrated by means of the position of the well-known 2^2S helium resonance at 19.37 eV (Buckman and Clark 1994) and the uncertainty in the energy is estimated to be within 0.20 eV. The overall energy resolution (FWHM) was typically 40 meV during these measurements. The true zero angle at every separate measurement has been determined according to the symmetry of the signal around the mechanical zero. The angular resolution was 1.5° at 20 eV and below this value at the higher energies considered.

The effective path length correction factors (Brinkman and Trajmar 1981) were determined for the present experimental conditions in which the DCSs decrease by three orders of magnitude. The measured angular distributions were averaged and then corrected using these factors to obtain relative DCSs. The absolute DCSs were obtained by normalization to the absolute DCSs of Register *et al* (1986) using the best agreement in shape. The errors include statistical errors, the normalization errors of 5% and the errors of the reference DCSs. The total errors, which were obtained as the root mean squares of the individual errors, are from 9 to 14%.

3. Theory

The use of an *ab initio* absorption potential within a relativistic framework is a new, and potentially very powerful, approach for electron collision processes. A complete development of the theory pertaining to the *ab initio* absorption potential, used in this work, will be given by Chen *et al* (2006) and hence only a very brief outline will be presented here.

The elastic scattering equations for the large and small components of the scattering wavefunction, namely $F_0(x)$ and $G_0(x)$, can be formulated in matrix form in terms of the integral equations

$$\begin{pmatrix} F_0(x) \\ G_0(x) \end{pmatrix} = \begin{pmatrix} v_1(k_0x) \\ v_2(k_0x) \end{pmatrix} + \frac{1}{k_0}\int_0^x \mathrm{d}r\, G^P_{\Gamma_0}(x,r) \times \left[U(r)\begin{pmatrix} F_0(r) \\ G_0(r) \end{pmatrix} - \begin{pmatrix} \overline{W}_P(\kappa_2;r) \\ \overline{W}_Q(\kappa_2;r) \end{pmatrix} - \mathrm{i}U^{\mathrm{I}}_{\mathrm{opt}}(r)\begin{pmatrix} F_0(r) \\ G_0(r) \end{pmatrix}\right] \tag{4}$$

where k_0 is the wave number of the incident electron and the local potential $U(r)$ is given by the sum of the static and a local polarization potential, i.e.,

$$U(r) = U_{00}(r) + U_{\mathrm{pol}}(r). \tag{5}$$

Furthermore, the imaginary part of the optical potential $U^{\mathrm{I}}_{\mathrm{opt}}(r)$ is given by

$$U^{\mathrm{I}}_{\mathrm{opt}}(x)\begin{pmatrix} F_0(x) \\ G_0(x) \end{pmatrix} = \sum\!\!\!\!\!\!\int_{\Gamma'}{}' \frac{1}{k_\nu} U_{0\Gamma'}(x)\int_0^\infty \mathrm{d}r\, U_{\Gamma'0}(r) G^{Q,I}_{\Gamma'}(x,r)\begin{pmatrix} F_0(r) \\ G_0(r) \end{pmatrix} \tag{6}$$

and is clearly non-local in character. Here, $k_{\nu'}$ is the wave number of the outgoing electron when the atom is left in a state specified by Γ'. In equation (4), the elements of the Green's function matrix $G^P_{\Gamma_0}(x,r)$ are defined in terms of the Riccati–Bessel and Riccati–Neumann functions according to

$$G^P_{ij}(x,r) = \bar{v}_i(k_0x)v_j(k_0r) - v_i(k_0x)\bar{v}_j(k_0r) \qquad \text{for} \quad i,j = 1,2 \tag{7}$$

where

$$v_1(k_0x) = \hat{\jmath}_{l_2}(k_0x) \qquad \bar{v}_1(k_0x) = \hat{n}_{l_2}(k_0x) \tag{8a}$$

$$v_2(k_0x) = s_{\kappa_2}\frac{\hbar c k_0}{\tilde{\epsilon}_0 + mc^2}\hat{\jmath}_{\bar{l}_2}(k_0x) \qquad \bar{v}_2(k_0x) = s_{\kappa_2}\frac{\hbar c k_0}{\tilde{\epsilon}_0 + mc^2}\hat{n}_{\bar{l}_2}(k_0x). \tag{8b}$$

Here, s_{κ_2} is the sign of κ_2, while $\bar{l}_2$ is given by $l_2 + 1$ when $\kappa_2 < 0$ and by $l_2 - 1$ when $\kappa_2 > 0$. Furthermore, the total relativistic energy of the incident electron is given by $\tilde{\epsilon} = m\gamma c^2$. The elements of the Green's function matrix in equation (6) are given by

$$G^{Q,I}_{ij}(x,r) = v_i(k_\nu x)v_j(k_\nu r) \qquad \text{for all} \quad r,x \qquad \text{for} \quad i,j = 1,2 \tag{9}$$

while the coupling potentials $U_{0\Gamma'}(x) = U_{\Gamma'0}(x)$ are defined by

$$U_{\Gamma'0}(x) = \frac{(1+\gamma)m}{\hbar^2}\langle \Psi_{\Gamma'}|V_x|\Psi_{\Gamma_0}\rangle. \tag{10}$$

Here, Ψ_{Γ_0} is the ground-state wavefunction of xenon while $\Psi_{\Gamma'}$ represents either a bound or continuum state of the atom. If $\Psi_{\Gamma'}$ is a bound state then its inclusion in the summation in equation (6) simulates excitation processes in the absorption potential while, if $\Psi_{\Gamma'}$ is a continuum state, then its inclusion in the integration in equation (6) simulates ionization processes. The bound-state wavefunctions for xenon were determined from the multiconfiguration Dirac–Fock code of Parpia *et al* (1996) while the continuum states were

Table 1. Differential cross sections for elastic electron scattering from xenon (in units of 10^{-16} cm^2 sr^{-1}) measured at CNU. Figures in parentheses indicate estimated percentage uncertainties.

	Energy (eV)				
Angle (°)	10	20	30	50	100
10		37.871(7)	18.027(8)	13.288(8)	14.109(7)
20	20.322(7)	19.425(7)	8.731(8)	2.880(9)	1.350(8)
30	12.808(7)	9.030(7)	3.510(7)	0.387(11)	0.078(15)
40	7.090(8)	3.211(8)	0.939(9)	0.036(16)	0.377(11)
50	3.500(8)	0.352(10)	0.132(10)	0.005(19)	0.250(12)
55		0.177(12)			
60	1.684(7)	0.264(12)	0.265(11)	0.014(17)	0.057(16)
65					0.009(15)
70	0.972(9)	0.700(11)	0.390(11)	0.031(16)	0.023(16)
80	0.711(8)	0.628(11)	0.294(11)	0.029(16)	0.101(13)
85			0.023(17)		
90	0.580(10)	0.273(11)	0.147(12)	0.041(17)	0.138(14)
95			0.129(13)		
100	0.479(9)	0.079(14)	0.151(12)	0.132(13)	0.072(13)
110	0.405(10)	0.116(13)	0.292(11)	0.266(13)	0.036(16)
120	0.517(11)	0.212(11)	0.300(11)	0.333(12)	0.055(15)
130	0.723(11)	0.190(11)	0.173(12)	0.254(12)	0.046(15)
140	1.221(10)	0.099(13)	0.030(16)	0.050(15)	0.006(20)
145			0.024(16)	0.011(16)	0.004(20)
150	2.010(10)	0.205(12)	0.401(13)	0.057(16)	0.025(17)
160	2.450(9)	0.351(11)	1.355(11)	0.573(12)	0.100(13)
170	2.938(8)	0.594(11)	2.650(11)	1.220(10)	0.211(12)
180	3.014(8)	0.855(10)	3.108(9)	2.007(9)	0.305(12)

determined numerically in the static field of the xenon ion. Finally, $\overline{W}_P$ and $\overline{W}_Q$ in equation (4) are the large and small components of the exchange interaction. Once again, the method of solution of these equations in order to obtain the complex phase shift η_κ has been detailed elsewhere (Chen *et al* 2006) and will not be repeated here.

In this work, the polarization potential included both static and dynamic multipoles up to and including $\nu = 6$ (Mimnagh *et al* 1993) while the coupling potential contained the following 15 bound states of xenon in the summation in equation (6), namely $6s[3/2]_1$, $6s[1/2]_1$, $6p[1/2]_0$, $6\bar{p}[1/2]_0$, $6p[5/2]_2$, $6\bar{p}[3/2]_2$, $6p[3/2]_2$, $5\bar{d}[1/2]_1$, $5d[3/2]_1$, $5\bar{d}[3/2]_1$, $5d[7/2]_3$, $5\bar{d}[5/2]_3$, $5d[5/2]_3$, $7s[3/2]_1$ and $7s[1/2]_1$, while the integration involved 15 continuum states corresponding to all possible partial waves from the s-wave, and up to and including, g-waves and $\bar{g}$-waves. We note that the total angular momentum of the states included in the optical potential are restricted due to parity conservation.

4. Results and discussion

The tabulated experimental results from CNU and the IOP-Belgrade are given in tables 1 and 2, respectively, and both experimental and theoretical results, together with some previous results, are presented in figures 1 and 2. For reasons of clarity in the plots, in figure 1 only the CNU results are compared with the previous experimental and theoretical results while in figure 2 all of the present experimental and theoretical results are presented. Even though the IOP results only extend up to 150° and not to 180°, they still cover a higher angular range than

Table 2. Differential cross sections for elastic electron scattering from xenon (in units of 10^{-16} cm^2 sr^{-1}) measured at the IOP-Belgrade. Figures in parentheses indicate estimated percentage uncertainties.

	Energy (eV)		
Angle (°)	20	30	50
10			20.053(11)
15	33.183(9)	26.688(11)	9.473(11)
20	24.711(10)	16.828(11)	3.971(11)
25	18.356(9)	10.156(11)	1.485(11)
30	11.426(9)	5.953(11)	0.471(12)
35	6.895(9)	2.572(11)	0.155(12)
40	3.130(9)	1.275(11)	0.0538(13)
45	1.318(9)	0.534(12)	0.0241(13)
50	0.347(10)	0.279(12)	0.0118(14)
54			0.0080(14)
55	0.159(10)	0.247(12)	0.0082(14)
60	0.287(10)	0.307(12)	0.0176(13)
65	0.544(10)	0.367(12)	0.0366(13)
70	0.770(10)	0.377(12)	0.0406(13)
75	0.800(10)	0.351(12)	0.0418(13)
80	0.753(10)	0.278(12)	0.0324(13)
84			0.0277(13)
85	0.567(10)	0.206(12)	0.0286(13)
90	0.333(10)	0.162(12)	0.0414(13)
93		0.154(12)	
95	0.178(10)	0.162(12)	0.0861(13)
100	0.0824(11)	0.220(12)	0.162(12)
105	0.0633(12)	0.291(12)	0.256(12)
110	0.0770(11)	0.348(12)	0.340(12)
115	0.151(10)	0.389(12)	0.403(12)
116		0.396(12)	
120	0.195(10)	0.364(12)	0.409(12)
125	0.204(10)	0.310(12)	0.376(12)
130	0.168(10)	0.244(12)	0.280(12)
135	0.110(10)	0.123(13)	0.188(12)
140	0.0810(11)	0.0470(13)	0.0831(13)
142		0.0231(14)	
144		0.0480(14)	
145	0.0976(11)	0.100(14)	0.0241(14)
149		0.270(14)	
150	0.187(10)		

other previous reports. We therefore have more backward angle cross sections with which to compare. In addition, the IOP measurements have smaller angular intervals around the DCS minima, where as the CNU measurements extend up to 180° in 10° intervals.

In general, the agreement between the earlier experimental works and the present measurements, in the angular range where they overlap, is good. However, the present calculations, with and without absorption effects included, show a varying degree of agreement with other calculations. From figure 2, it is clear that the best agreement between the CNU experiments and the present theory is obtained with the calculation that includes absorption effects. However, at small angles, where absorption effects are not important, both theories are in excellent agreement with experiment for the energies considered. The neglect of absorption

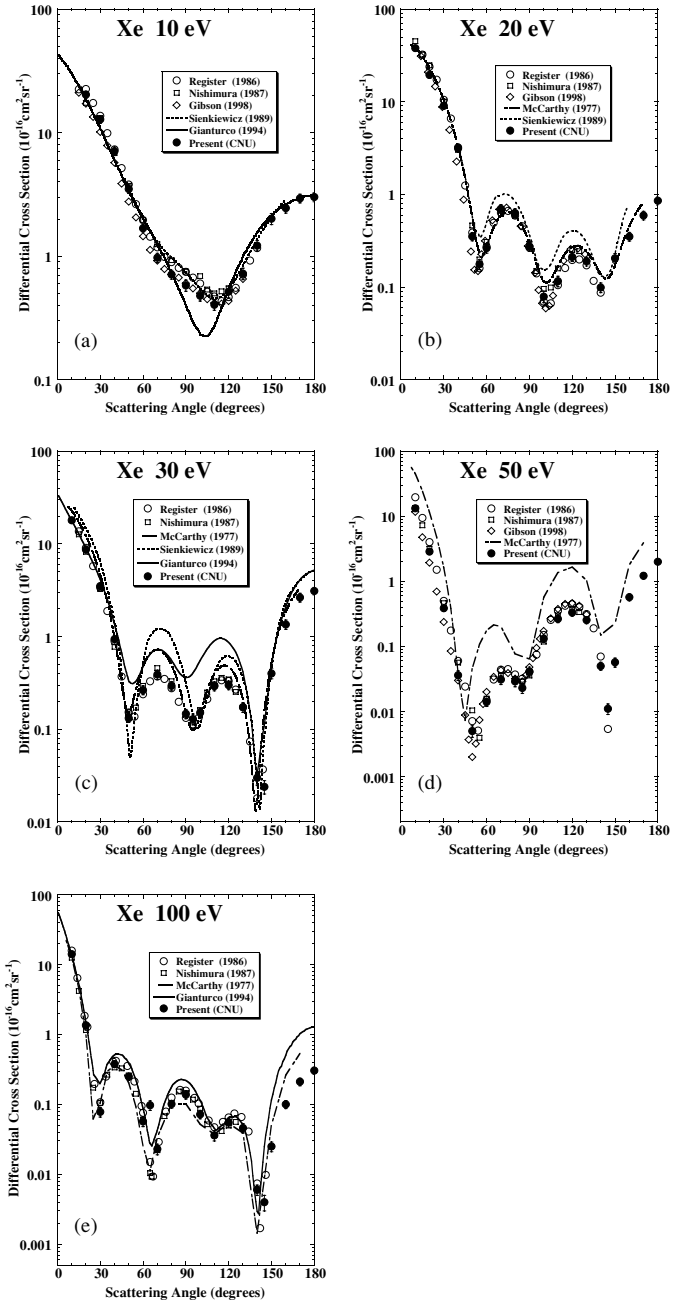

Figure 1. Absolute differential cross sections for elastic electron scattering from xenon at (a) 10 eV, (b) 20 eV, (c) 30 eV, (d) 50 eV and (e) 100 eV. Experimental: (●) present CNU results, (○) Register *et al* (1986), (□) Nishimura *et al* (1987), (◇) Gibson *et al* (1998). Theoretical: (– – –) Sienkiewicz and Baylis (1989), (——) Gianturco and Rodriguez-Ruiz (1994), (– —) McCarthy *et al* (1977).

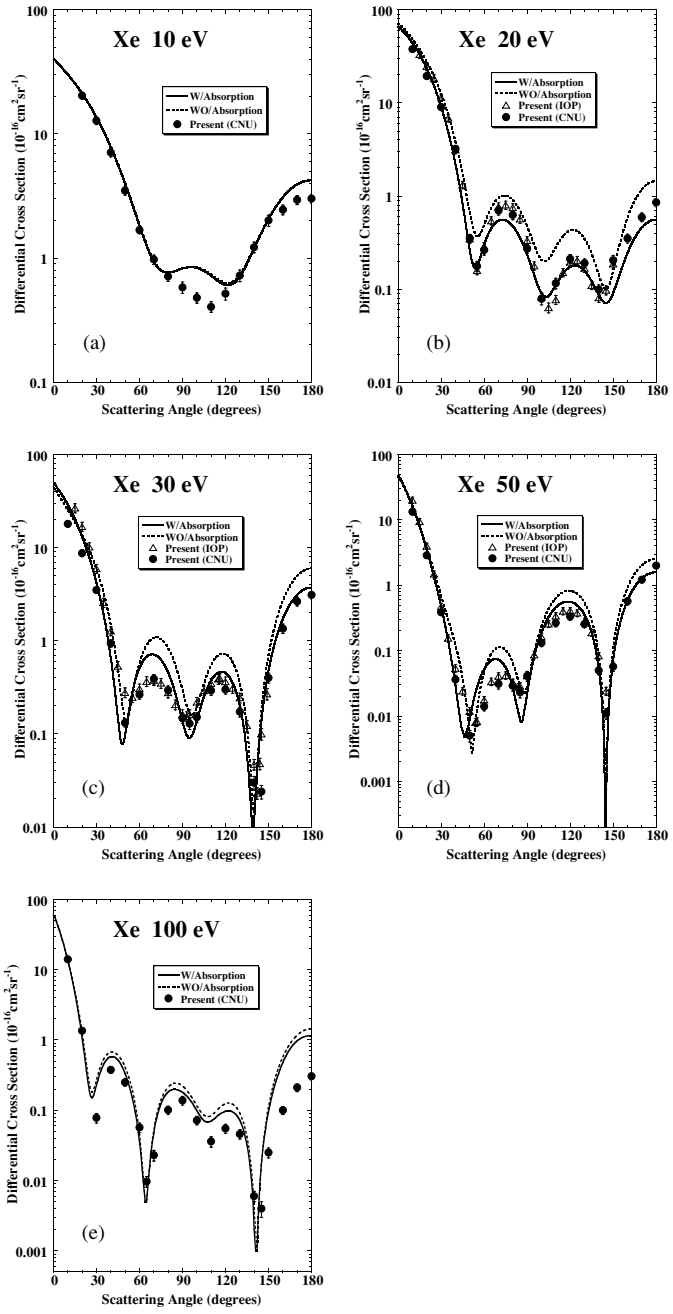

Figure 2. Absolute differential cross sections for elastic electron scattering from xenon at (a) 10 eV, (b) 20 eV, (c) 30 eV, (d) 50 eV and (e) 100 eV. Experimental: (△) present IOP-Belgrade results, (●) present CNU results. Theoretical: (——) present calculation with absorption, (– – –) present calculation without absorption.

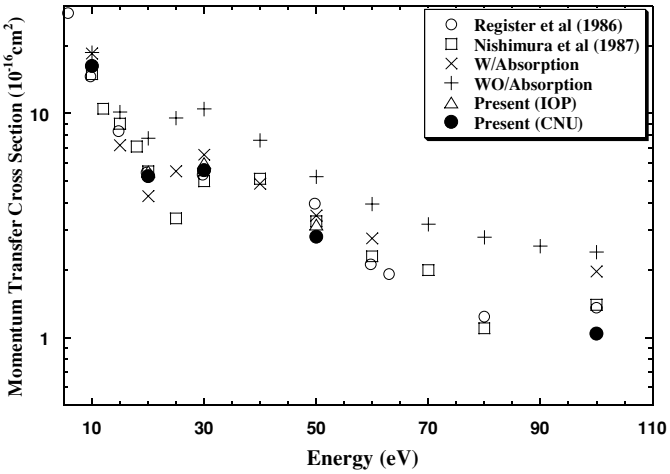

Figure 3. The momentum transfer cross section versus the incident electron energy. Experimental: (○) Register *et al* (1986), (□) Nishimura *et al* (1987), (△) present IOP-Belgrade results, (●) present CNU results. Theoretical: (×) present calculation with absorption, (+) present calculation without absorption.

Table 3. Momentum transfer cross sections (in units of 10^{-16} cm^2) of the present experimental (CNU and IOP-Belgrade) and theoretical results at the electron energies where the elastic differential cross sections are measured.

	Energy (eV)				
	10	20	30	50	100
Present (CNU)	16.292	5.243	5.579	2.817	1.041
Present (IOP)		5.503	5.999	3.189	
With absorption	18.502	4.268	6.536	3.502	1.969
Without absorption	18.681	7.736	10.467	5.221	2.407

results in a cross section which is too high at almost all scattering angles. This is particularly true at backward scattering angles where the present differential cross sections are in good agreement with the theoretical calculations which include absorption, except at 10 and 100 eV. At 10 eV, which is barely above the first inelastic threshold of the $6s[3/2]_2$ state at 8.315 eV for xenon, the overall agreement is not good. At 100 eV, the present theory predicts a much higher cross section at backward angles than the present experiments. The same is true, but to a lesser extent, for the theoretical calculation of McCarthy *et al* (1977) in figure 1(e). In general, the *ab initio* and non-local model of Chen *et al* (2006) is in best overall agreement with the optical model calculations of McCarthy *et al* (1977) which contained a local absorption potential while our results without absorption are closer to the calculations of Sienkiewicz and Baylis (1989). Nonetheless, the current model does not yield as much absorption for xenon as the model of McCarthy *et al*. However, it must be remembered that, in the latter case, this model contains a parameter which is adjusted to yield the total experimental cross section (elastic plus inelastic). The model of Chen *et al* only includes direct excitation and outer shell ionization processes in the determination of the inelastic cross section. At the lower energies considered here, excitation processes which occur via exchange will also be important, while at the higher energies, inner shell ionization processes will also contribute to the inelastic cross section.

The momentum transfer cross section is more suitable than the integral cross section to test the validity of the present results since the DCS is then multiplied by the factor $(1-\cos\theta)$ which is greatest at large scattering angles. The momentum transfer cross sections determined from the present experimental measurements and theoretical calculations are presented in table 3 and figure 3 where they are compared with the results of Register *et al* (1986) and Nishimura *et al* (1987). The local minimum around 20 eV is evident in all cases, except for the data of Nishimura *et al*, with very good agreement in the absolute values. One can see that a substantial improvement in the agreement between theory and experiment is obtained when absorption effects are included in the calculation.

5. Conclusions

We have presented, for the first time, measurements of the elastic DCSs at intermediate energies for xenon over effectively the entire angular range, namely up to 180°. We have also presented experimental and theoretical values for the momentum transfer cross section in this energy range. It is apparent that the theoretical treatment of intermediate energy elastic scattering from xenon is sensitive to the inclusion of absorption effects, particularly at backward scattering angles. This observation plus the results for the krypton case (Cho *et al* 2004) indicates that the role of absorption is generally quite important for the rare gases.

Acknowledgments

This work was supported by the KRF (2004-042-C00029) and MNZZS No 141011. Some of the collaborative aspects were supported by the grants from the Core University Program (JSPS and KOSEF) and from the Australian Research Council's Linkage Programme.

References

Boesten L and Tanaka H 1992 *At. Data Nucl. Data Tables* **52** 25
Brinkmann R T and Trajmar S 1981 *J. Phys. E: Sci. Instrum.* **14** 245
Buckman S J and Clark C W 1994 *Rev. Mod. Phys.* **66** 539
Chen S, McEachran R P and Stauffer A D 2006 *J. Phys. B: At. Mol. Opt. Phys.* **39** at press
Cho H, Lee H and Park Y S 2003a *Radiat. Phys. Chem.* **68** 115
Cho H, Lee H and Park Y S 2003b *J. Korean Phys. Soc.* **43** 40
Cho H, McEachran R P, Tanaka H and Buckman S J 2004 *J. Phys. B: At. Mol. Opt. Phys.* **37** 4639
Ester T and Kessler J 1994 *J. Phys. B: At. Mol. Opt. Phys.* **27** 4295
Gianturco F A and Rodriguez-Ruiz J A 1994 *Z. Phys.* D **31** 149
Gibson J C, Lun D R, Allen L J, McEachran R P, Parcell L A and Buckman S J 1998 *J. Phys. B: At. Mol. Opt. Phys.* **31** 3949
Johnson W R and Guet C 1994 *Phys. Rev.* A **49** 1041
McCarthy I E, Noble C J, Phillips B A and Turnbull A D 1977 *Phys. Rev.* A **15** 2173
McEachran R P and Stauffer A D 1990 *J. Phys. B: At. Mol. Opt. Phys.* **23** 4605
Mimnagh J R, McEachran R P and Stauffer A D 1993 *J. Phys. B: At. Mol. Opt. Phys.* **26** 1727
Nishimura H, Matsuda T and Danjo A 1987 *J. Phys. Soc. Japan* **56** 70
Parpia F A, Froese-Fischer C and Grant I P 1996 *Comput. Phys. Commun.* **94** 249
Read F H and Channing J M 1996 *Rev. Sci. Instrum.* **67** 2372
Register D F, Vuskovic L and Trajmar S 1986 *J. Phys. B: At. Mol. Phys.* **19** 1685
Sienkiewicz J E and Baylis W E 1989 *J. Phys. B: At. Mol. Opt. Phys.* **22** 3733
Srivastava S K, Chutjian A and Trajmar S 1975 *J. Chem. Phys.* **63** 2659